





Article

# Comparison of the Flexural Behavior of High-Volume Fly Ash Based Concrete Slab Reinforced with GFRP Bars and Steel Bars

Chinnasamy Samy Madan<sup>1</sup>, Swetha Munuswamy<sup>1</sup>, Philip Saratha Joanna<sup>1,\*</sup> ,  
Beulah Gnana Ananthi Gurupatham<sup>2</sup> and Krishanu Roy<sup>3,\*</sup> 

<sup>1</sup> Department of Civil Engineering, Hindustan Institute of Technology and Science, Padur, Chennai 603103, India; chinna\_3\_2001@yahoo.com (C.S.M.); swethamunus@gmail.com (S.M.)

<sup>2</sup> Department of Civil Engineering, Anna University, Chennai 600025, India; beulah28@annauniv.edu

<sup>3</sup> School of Engineering, Civil Engineering, The University of Waikato, Hamilton 3216, New Zealand

\* Correspondence: joanna@hindustanuniv.ac.in (P.S.J.); krishanu.roy@waikato.ac.nz (K.R.)

**Abstract:** Fiber-reinforced polymer (FRP) rods are advanced composite materials with high strength, light weight, non-corrosive properties, and superior durability properties. Under severe environmental conditions, for concrete structures, the use of glass-fiber-reinforced polymer (GFRP) rods is a cost-effective alternative to traditional steel reinforcement. This study compared the flexural behavior of an OPC concrete slab with a high-volume fly ash (HVFA) concrete slab reinforced with GFRP rods/steel rods. In the fly ash concrete slabs, 60% of the cement used for casting the slab elements was replaced with class F fly ash, which is emerging as an eco-friendly and inexpensive replacement for ordinary Portland cement (OPC). The data presented include the crack pattern, load–deflection behavior, load–strain behavior, moment–curvature behavior, and ductility of the slab specimens. Additionally, good agreement was obtained between the experimental and nonlinear finite element analysis results using ANSYS 2022-R1. The study also compared the experimental moment capacity with the most commonly used design standard ACI 440.1R-15. This investigation reveals that there is a huge potential for the utilization of GFRP rods as reinforcement in fly ash concrete slabs.

**Keywords:** glass-fiber-reinforced polymer (GFRP) rods; concrete slab; high-volume fly ash; moment–curvature; ductility



**Citation:** Madan, C.S.; Munuswamy, S.; Joanna, P.S.; Gurupatham, B.G.A.; Roy, K. Comparison of the Flexural Behavior of High-Volume Fly Ash Based Concrete Slab Reinforced with GFRP Bars and Steel Bars. *J. Compos. Sci.* **2022**, *6*, 157. <https://doi.org/10.3390/jcs6060157>

Academic Editor: Francesco Tornabene

Received: 2 May 2022

Accepted: 24 May 2022

Published: 26 May 2022

**Publisher's Note:** MDPI stays neutral with regard to jurisdictional claims in published maps and institutional affiliations.



**Copyright:** © 2022 by the authors. Licensee MDPI, Basel, Switzerland. This article is an open access article distributed under the terms and conditions of the Creative Commons Attribution (CC BY) license (<https://creativecommons.org/licenses/by/4.0/>).

## 1. Introduction

Sustainability is an important factor for the well-being and continuous growth of society. The reduction in CO<sub>2</sub>, the main ingredient of greenhouse gases, has become critical for ensuring a sustainable ecosystem. Cement is the prime ingredient in concrete, and its production leads to 7 to 10% of global carbon emissions. Because of its pozzolanic properties, fly ash can be utilized as a cement substitute in concrete slab elements. The pozzolanic properties of fly ash suggest that it could be utilized as a cement substitute in slab elements. Green concrete is becoming more popular in the construction business because of the disadvantages of traditional concrete. The various green concrete types available are geopolymer concrete, ultrahigh performance concrete, high-volume fly ash concrete, and lightweight concrete [1,2].

Fly ash has become an important ingredient in concrete, as the spherical shape of fly ash helps in improving the workability of fresh concrete, and its smaller particle size helps it fill voids in the concrete, leading to the production of dense and durable concrete. Class F fly ash is widely used by the construction industry [3–5]. Reinforced concrete (RC) beams can be prepared, which contain 50% fly ash instead of cement [6]. High-volume fly ash (HVFA) concrete, in which 60% of cement was replaced with fly ash, showed excellent mechanical properties with enhanced durability performance. Replacing 60% of cement

with fly ash can produce adequate strength in self-compacting concrete [7]. Concrete containing up to 60% fly ash plus a chemical superplasticizer can be adjusted to meet structural-grade concrete strength and workability criteria. The early-age compressive strength of fly ash concrete was less than that of the control concrete, but the strength of the fly ash concrete gradually improved over a long period due to the pozzolanic reaction. However, the strong growth of control samples stopped after 56 days of curing [8–10].

In concrete structures, the use of non-metallic FRP reinforcement as an alternative to steel reinforcement is gaining acceptance due to its resistance to corrosion and its better mechanical properties. FRP composites have the advantage of high strength, light weight, and corrosion resistance and are considered for rehabilitation and strengthening purposes in concrete structural members [11].

The FRP rod assures better long-term performance than steel reinforcement [12]. Shave [13] suggested that to prevent corrosion, FRP rods can be used instead of steel reinforcement in precast concrete structures. Nowadays, the use of FRP is still not widespread despite its high potential for application in the field of civil engineering and the advantages it provides as an alternative to steel bars. One of the reasons for this may be the lack of design codes for the design of FRP structures.

GFRP rods can be used to improve the structural response of existing flat slabs and also to withstand higher longitudinal strains. They also provide remediation for punching shear failure [14]. The HVFA concrete element with GFRP composites could provide better fire protection up to 1100 °C [15]. In addition, the use of a flame retardant and nanoparticles on the fiber composite can improve the mechanical properties of the GFRP composite, which can also significantly improve the lifespan [16–21]. The fiber composite also showed promising electrical conductivity, a positive effect on the post-fracture residual stiffness, redundancy, resistance, load-bearing capacity, and flexural strength of structural beams [22–24].

The crack width limitations for reinforced concrete (RC) elements reinforced with FRP rods are more relaxed than for RC elements reinforced with steel rods. Less severe crack width limits could be adopted, as FRP bars are corrosion-resistant [25]. When the whole-life cost of GFRP bars is considered, they provide an economical solution, reduce maintenance costs, and increase the useful life of the structure. The installation of GFRP rods in structural elements is similar to that of steel rods, along with fewer handling, transporting, and storage problems [26–28]. As GFRP bars are anisotropic composite materials, they have higher tensile strength. The yield tensile strength of GFRP bars is 13% higher than that of steel rebar. The yield strain of the GFRP bar is 58% higher than that of steel rebar [29]. Research carried out on concrete structural elements reinforced with GFRP rods showed no reaction or degradation process in the presence of an alkaline and corrosive environment [30]. The mechanical properties of GFRP rods were better than those of the conventional steel reinforcement, and the GFRP rods provided good resistance against environmental effects such as a chemical attack, freeze–thaw cycles, etc. [31,32]. The flexural behavior of a beam reinforced with glass-fiber-reinforced polymer as an alternative to traditional steel reinforcement was studied. The results showed that GFRP rods had flexural behavior similar to that of steel rods. Besides acceptable shear properties, concrete elements reinforced with GFRP rods led to high bending properties [33,34].

A nonlinear finite element (NLFE) model using ANSYS software was used to investigate the structural performance of concrete elements reinforced with GFRP bars. The effects of the ultimate load, ultimate deflection, crack pattern, stress, strain, and displacement of concrete elements with different end conditions can be analyzed in ANSYS [35–37].

Only a few research works have been carried out with green concrete reinforced with GFRP rods. The present study compares the flexural behaviors of HVFA-based concrete slab and OPC concrete slab reinforced with GFRP rods and steel rods. Comparisons were made in terms of crack pattern, load–deflection behavior, load–strain behavior, ultimate moment capacity, and ductility. ANSYS 2022-R1 [38] software was used to investigate the structural performance in terms of the ultimate load and deflection of concrete slabs

reinforced with steel/GFRP bars. The study also compared the experimental moment capacity with the most commonly used design standard ACI 440.1R-15.

## 2. Materials and Methods

### 2.1. Concrete

The materials used in the concrete mix were ordinary Portland cement of 53 grade, class F fly ash, manufactured sand as fine aggregate, gravel as coarse aggregate, 10% micro silica by weight of the binder, and 0.3% superplasticizer (Master Glenium sky 8233). The water–cement ratio adopted was 0.5. M25 grade concrete was used to cast the slabs. The properties of class F fly ash are given in Table 1. The compressive strength of the cube and the split tensile strength of the cylinder with OPC concrete and HVFA concrete after 28 days and 56 days of curing are shown in Table 2.

**Table 1.** Properties of fly ash (class F).

Chemical Composition	Content (% by Mass)
SiO <sub>2</sub>	52.52
Al <sub>2</sub> O <sub>3</sub>	32.63
Fe <sub>2</sub> O <sub>3</sub>	6.16
CaO	Nil
NA1-20	0.02
SO <sub>3</sub>	4.95
MnO	0.03
LOI	1.08

**Table 2.** Strength of Concrete.

Specimen Type	Compressive Strength $f'_c$ (MPa)		Split Tensile Strength (MPa)	
	28 Days	56 Days	28 Days	56 Days
Control concrete	34.23	36.27	3.94	5.01
60% Fly ash concrete	26.39	37.74	3.16	5.79

### Reinforcing Bars

The GFRP rods used in the slabs were manufactured as per ACI 440.6M-08 and ACI 440.3R-04. The steel rods used as reinforcement in the slab specimens were of Fe550D grade. The tests were performed by the manufacturers following the ASTM D7205/D7205M-06 standards, and the mechanical properties of the GFRP rod and steel rod were determined. The mechanical properties of steel and GFRP rods are shown in Table 3. The GFRP rod used in the experiment is shown in Figure 1.

**Table 3.** Mechanical properties of steel and GFRP rods.

Reinforcement Material	Diameter (mm)	Tensile Strength $f_{fu}$ (MPa)	Modulus of Elasticity $E_f$ (MPa)	Density (Kg/m <sup>3</sup> )
STEEL rod	10	650	200,000	7800
GFRP rod	10	1100	55,000	1900

### 2.2. Experimental Program

#### 2.2.1. Specimen Details

The experimental program consisted of four groups: OPC concrete slab with steel bars, OPC concrete slab with GFRP bars, HVFA concrete slab with steel bars, and HVFA concrete slab with GFRP bars. A total of eight slabs were tested, with two slabs in each group. All of the one-way slab specimens had a span of 1000 mm, a width of 450 mm, and a depth of 100 mm. The slabs were reinforced with GFRP/steel rods with a center–center spacing of 130 mm along the longer span and 240 mm along the shorter span. In the high-volume fly

ash concrete slab, 60% of cement was replaced with fly ash (class F). All specimens were tested on the 56th day from the date of casting. A four-letter designation was given to the slab specimens. The first two letters refer to reinforcement type, which may take the value SR or GR: SR for steel reinforcement and GR for GFRP rods. The third letter indicates the type of concrete (C, F): C for OPC concrete and F for high volume fly ash concrete. The fourth identifier represents the trial number of the specimens in a particular series, as two specimens were tested in each series. The tested specimen details are given in Table 4.



**Figure 1.** Photograph of GFRP rods.

**Table 4.** Details of Test Specimens.

Specimen	Concrete Material	Reinforcement Material	Diameter (mm)
SRC	OPC (C)	Steel rod (SR)	10
SRF	Fly ash (F)	Steel rod (SR)	10
GRC	OPC (C)	GFRP rod (GR)	10
GRF	Fly ash (F)	GFRP rod (GR)	10

### 2.2.2. Experimental Setup

The RC slabs were tested in a loading frame with a capacity of 40 T. One end of the slab rested on the hinge support, and the other end rested on the roller support with an effective span of 800 mm. A spreader beam was used to apply two-point loading on the slab element. Static loads were applied to the slab specimen through the load cell. The deflections of the slabs were measured by linear voltage displacement transducers (LVDTs). An internal strain gauge was pasted on the surface of the steel/GFRP reinforcements with precaution during the casting of slabs to measure the tensile strain. For measuring the compressive strain, the strain gauge was pasted externally on the top surface of the slabs at the time of testing. The signals obtained from the LVDT and the electrical strain gauges were captured by a data acquisition system, which in turn was connected to a computer. The load was gradually applied with an increment of 2 kN/min until the failure of the slabs. The experimental setup for testing the slab is shown in Figure 2.

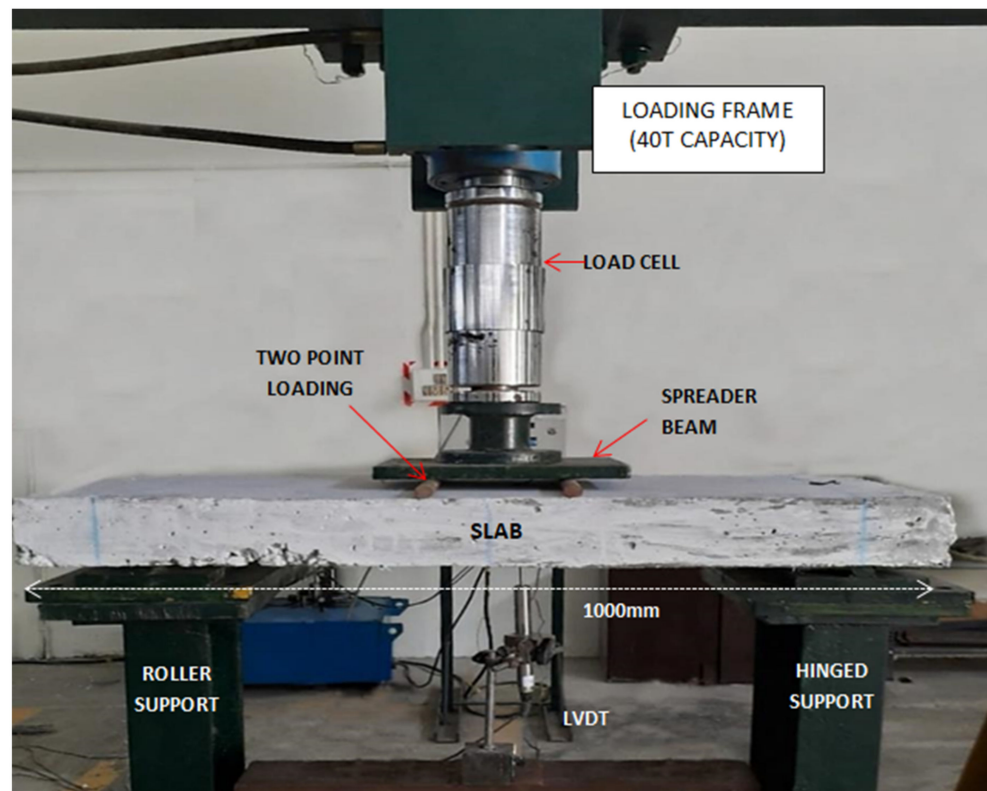


Figure 2. Experimental setup.

### 3. Results and Discussion

#### 3.1. Crack Pattern

The typical crack patterns of the SRC and SRF slabs are shown in Figures 3 and 4, respectively, and the crack patterns of the GRC and GRF slabs are shown in Figures 5 and 6, respectively. The crack patterns and the modes of failure are similar in slabs with steel bars and GFRP bars [39]. All tested slabs were initially uncracked before loading, and the first cracking of slabs occurred in the constant moment region. The average first crack loads in SRC, SRF, GRC, and GRF slabs were 16 kN, 18.8 kN, 15.75 kN, and 18.05 kN, respectively. After the first cracking, new cracks were formed in the slabs, and the width of the existing cracks continued to enlarge with the load increment in all of the slabs. At the ultimate load, cracks from the bottom of the slabs propagated to the top surface of the slabs. In all slabs, the cracks were mainly vertical flexural cracks that were perpendicular to the longitudinal axis of the slabs. All slabs failed due to the crushing of the concrete at the top surface of the slabs, and no failure was noticed in the steel bars and GFRP bars. Table 5 shows the first crack load and the ultimate load of all the slabs.

Table 5. First crack load and ultimate load of slab reinforced with steel and GFRP rods.

Specimen ID	First Crack Load $P_{cr}$ (kN)	Ultimate Load $P_u$ (kN)
SRC 1	15.7	24
SRC 2	16.3	23.8
SRF 1	19.1	28.5
SRF 2	18.5	27.3
GRC1	15.2	29
GRC2	16.3	28.1
GRF 1	17.6	31.8
GRF 2	18.5	30.3

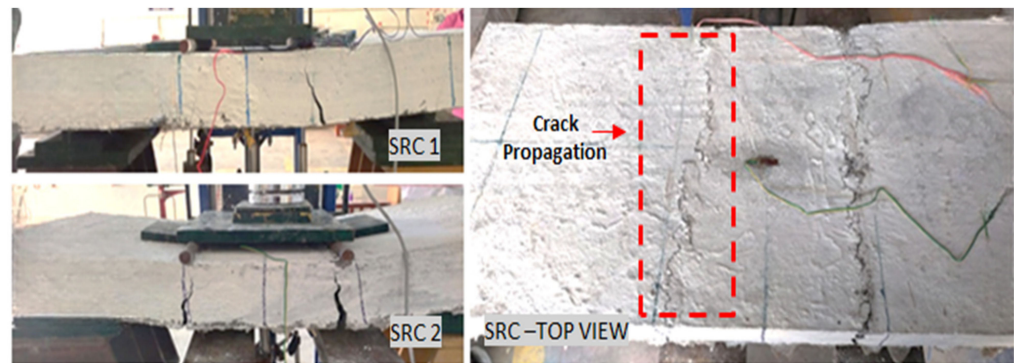


Figure 3. Crack pattern and failure mode of SRC slab.

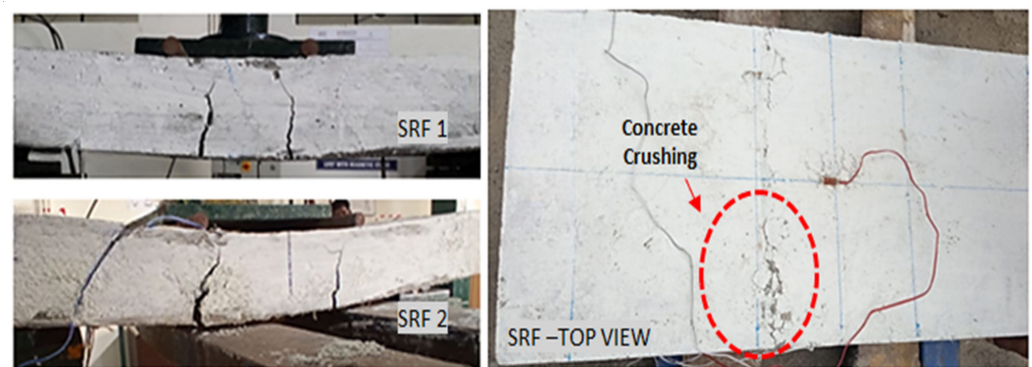


Figure 4. Crack pattern and failure mode of SRF slab.

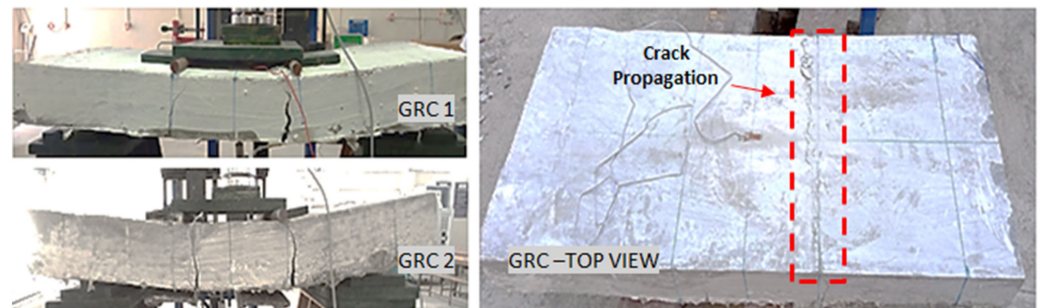


Figure 5. Crack pattern and failure mode of GRC slab.

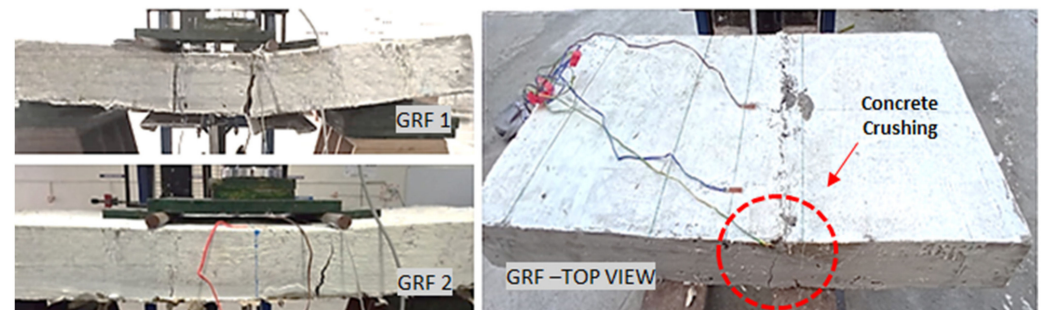


Figure 6. Crack pattern and failure mode of GRF slab.

### 3.2. Load–Deflection Behavior

The load–deflection behaviors of OPC and 60% fly ash concrete slabs reinforced with steel rods are shown in Figure 7, and those of OPC and 60% fly ash concrete slabs reinforced with GFRP rods are shown in Figure 8. The average ultimate load-carrying capacities of

the concrete slab specimens SRC, SRF, GRC, and GRF were 23.9 kN, 27.9 kN, 28.55 kN, and 31.05 kN, respectively. The slab specimens SRF, GRC, and GRF showed 16.7%, 19.4%, and 29.9% increases in the ultimate load-carrying capacity when compared with the control specimen SRC [40]. The comparison of the ultimate load of slab specimens is shown in Figure 9. In the OPC concrete slab and fly ash concrete slab reinforced with steel rods, the initial loading phase corresponds to elastic behavior, in which no cracking appeared. A drop in the slope of the curve was observed after the cracking load due to progressive crack formation in the slab, and an almost linear segment was observed until failure. Steel-reinforced slabs and GFRP-reinforced slabs failed due to the crushing of concrete. In the concrete slab reinforced with GFRP rods, the deflection continued to increase with the increase in load and exhibited some ductility even though GFRP has a brittle nature [41].

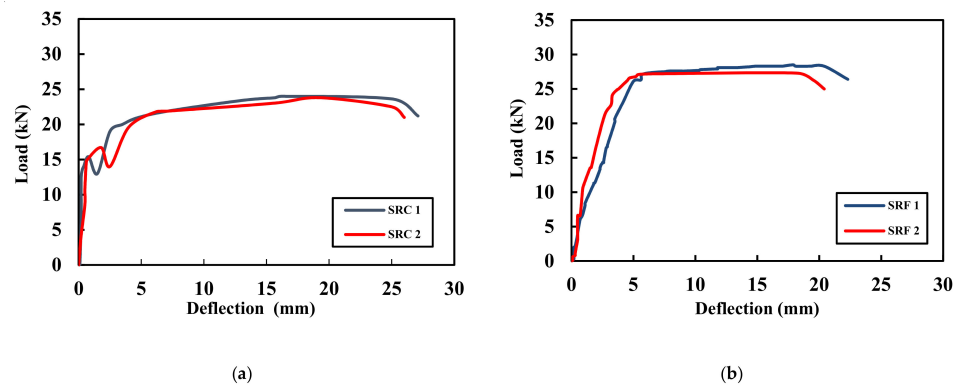


Figure 7. Load–deflection behavior of (a) SRC and (b) SRF.

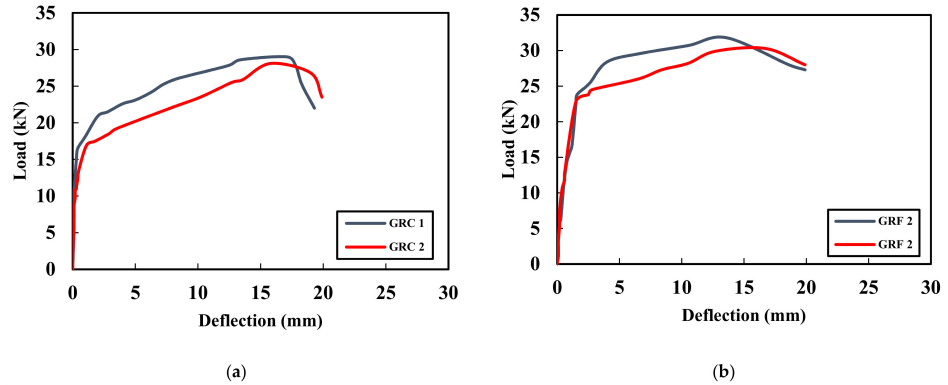


Figure 8. Load–deflection behavior of (a) GRC and (b) GRF.

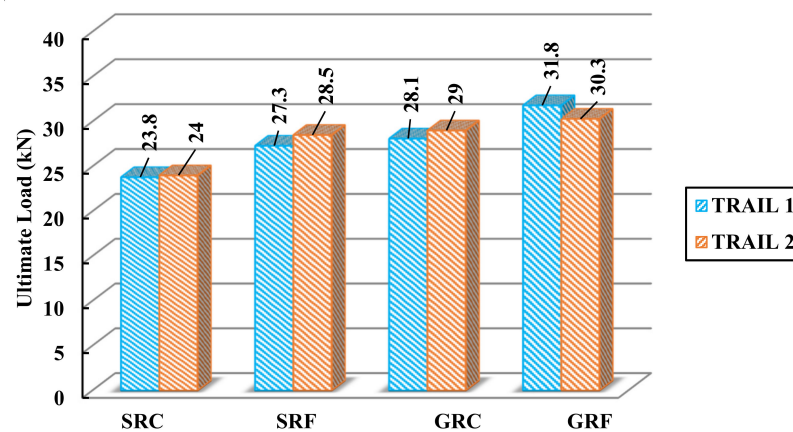


Figure 9. Comparison of ultimate load of the slab specimens.

### 3.3. Strain Distribution

The strain in OPC and fly ash concrete slabs at the top and bottom reinforcement was measured at the mid-span of the specimens. The positive strain represents the strain on the top surface of the OPC/fly ash concrete, and the negative strain represents the strain values of the steel rods/GFRP rods. The load–strain curves for SRC and SRF are shown in Figure 10, and the load–strain curves for GRC and GRF are shown in Figure 11. The strain in the steel rod and GFRP rod of the OPC concrete slab was  $19,577 \times 10^{-6}$  mm/mm and  $23,378 \times 10^{-6}$  mm/mm, respectively. The strain in the steel rod and GFRP rod of the fly ash concrete slab was  $21,075 \times 10^{-6}$  mm/mm and  $23,845 \times 10^{-6}$  mm/mm, respectively. The ultimate strain at the top of the OPC/fly ash concrete slabs lay in the range of 0.28% to 0.31% for the slab with steel reinforcement, and it ranged from 0.30% to 0.33% for the slab with GFRP reinforcement. The strain in the GFRP rods was higher than in steel rods in the OPC and fly ash concrete slab. From the graph, it can be observed that the concrete slab reinforced with GFRP rods has higher flexural strength than the steel-reinforced concrete slab [29,42].

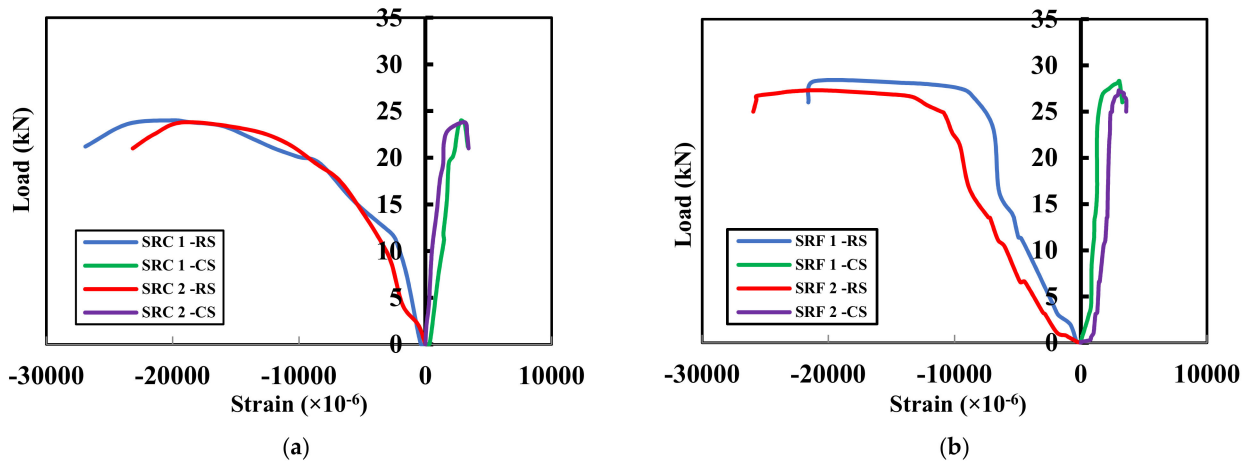


Figure 10. Load–strain behavior of (a) SRC and (b) SRF. RS—reinforcement strain; CS—concrete strain.

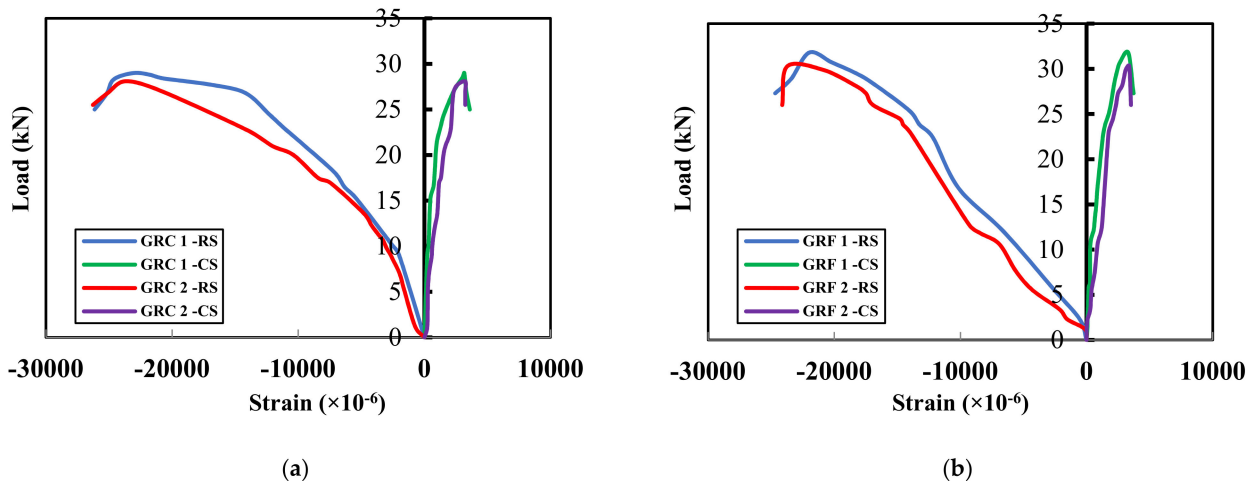


Figure 11. Load–strain behavior of (a) GRC and (b) GRF. RS—reinforcement strain; CS—concrete strain.

### 3.4. Moment–Curvature

The moment–curvature behaviors of the OPC and fly ash concrete slabs reinforced with steel rods are shown in Figure 12, and those of the OPC and fly ash concrete slabs reinforced with GFRP rods are shown in Figure 13. The moment vs. curvature relationship reflects ductility as well as provides the macroscopic mechanical properties of the slab elements.



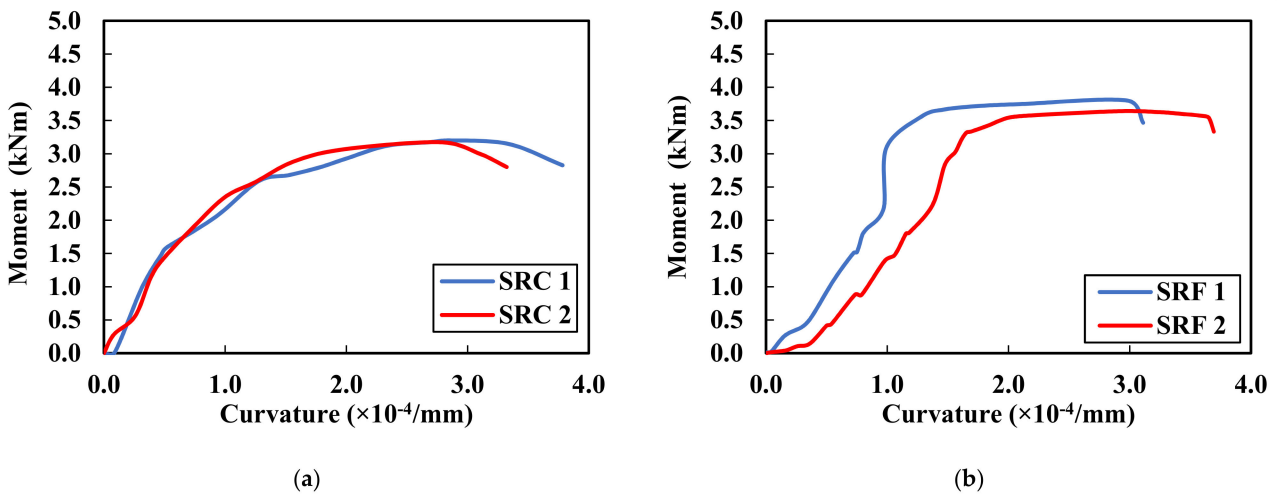


Figure 12. Moment–curvature behavior of (a) SRC and (b) SRF.

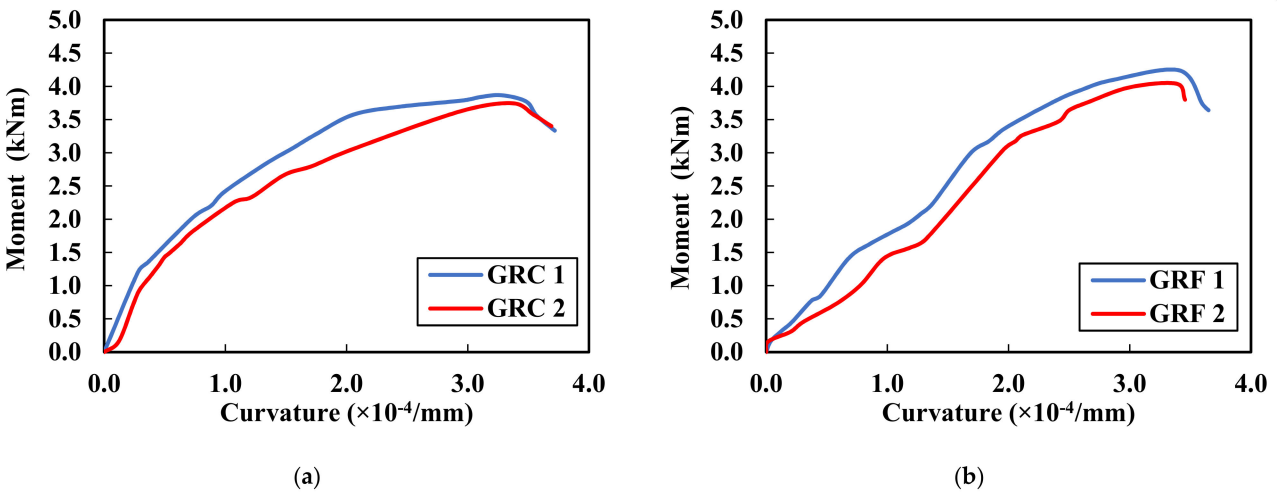


Figure 13. Moment–curvature behavior of (a) GRC and (b) GRF.

The curvature ( $\varnothing$ ) was calculated using the following Equation (1):

$$\varnothing = \frac{\varepsilon_c + \varepsilon_r}{d} \tag{1}$$

where  $\varepsilon_c$  is the compressive strain in concrete,  $\varepsilon_r$  is the tensile strain in the reinforcement (steel/GFRP rod), and  $d$  is the effective depth of the slab.

The average ultimate moment capacities of the SRC, SRF, GRC, and GRF slabs were 3.18 kNm, 3.67 kNm, 3.81 kNm, and 4.12 kNm, respectively. The ultimate moment capacity of the GRF slab was 12% higher than that of the SRF slab, and the ultimate moment capacity of the GRC slab was 20% higher than that of the SRC slab. The provision of GFRP rods increased the slab curvature capacity more than the steel rods at the same moment. In a concrete slab reinforced with steel rods, the moment capacity was sustained with an increase in curvature before failure, but the slab reinforced with GFRP rods attained the peak moment capacity just before failure. However, it can be noted that slabs reinforced with GFRP rods are capable of exhibiting more curvature before failure when compared to slabs reinforced with steel rods [43]. The ultimate moment capacity of the tested slabs is provided in Table 6.

**Table 6.** Performance details of the slabs reinforced with steel rods and GFRP rods.

Slab Designation	Max. Load ( $P_u$ ) (kN)	Deflection at Max Load ( $\Delta$ ) (mm)	Ultimate Moment ( $M_{Exp}$ ) (kNm)	Ultimate Strain in Concrete ( $\epsilon_{cu}$ ) %	Ultimate Strain In Reinforcement ( $\epsilon_f$ ) %	Ductility Ratio
SRC 1	24.0	16.2	3.20	0.28	2.00	11.77
SRC 2	23.8	19.2	3.17	0.31	1.90	11.87
SRF 1	28.5	17.9	3.70	0.30	2.19	12.27
SRF 2	27.3	18.2	3.64	0.30	2.02	11.33
GRC 1	29.0	17.1	3.87	0.31	2.30	7.33
GRC 2	28.1	15.8	3.75	0.32	2.36	7.72
GRF 1	31.8	13.6	4.24	0.33	2.39	8.35
GRF 2	30.3	16.7	4.04	0.33	2.37	7.88

### 3.5. Displacement Ductility

Displacement ductility is defined as the ratio of ultimate deflection to first yield deflection [44]. A high ductility ratio implies that a structural member is capable of undergoing a large deflection before failure. The ductility calculation for both the steel-reinforced concrete slab and GFRP-reinforced concrete slab is shown in Figure 14. Despite the brittle nature of the GFRP composites, these GFRP rods showed ductility in the concrete slab [45]. The SRF and GRF slabs had an average ductility of 11.8 and 8.1, respectively, and the average ductility of SRC and GRC was 11.5 and 7.52, respectively. Since the ductility of GFRP rods is above 4, they can be used in structural members [6]. Both the slabs reinforced with steel and GFRP rods failed due to flexure with maximum strength and ductility, whereas the SRC and SRF slabs showed greater ductility than the GRC and GRF slabs. The ductility of the tested slabs is provided in Table 6.

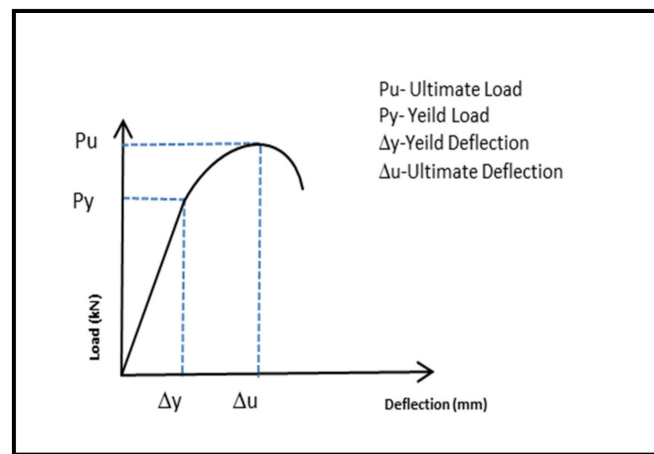


Figure 14. Displacement Ductility (Thamrin et al. [44]).

## 4. Theoretical Prediction

### 4.1. Equations Provided by ACI 44.1R-15

In this study, the theoretical flexural capacities ( $M_u$ ) of steel-rod- and GFRP-rod-reinforced concrete slabs were computed based on the equations provided by ACI 440.1R-15 [25,46]. According to ACI 440.1R-15, the moment of resistance of a concrete slab reinforced with GFRP rods can be determined based on the internal force equilibrium, strain compatibility, and the controlling mode of failure. The predicted failure mode can be determined by comparing the reinforcement ratio in Equation (2) to the balanced reinforcement ratio in Equation (3).

$$\rho_f = \frac{A_f}{bd} \tag{2}$$

where  $A_f$  is the area of GFRP rods,  $b$  is the width of the cross-section, and  $d$  is the distance from the extreme compression fiber to the centroid of the GFRP rods.

$$\rho_{fb} = 0.85\beta_1 \frac{f'_c}{f_{fu}} \frac{E_f \epsilon_{cu}}{E_f \epsilon_{cu} + f_{fu}} \tag{3}$$

where  $f'_c$  is the specified compressive strength of concrete,  $f_{fu}$  is the ultimate tensile stress of GFRP bars,  $E_f$  is the elastic modulus of GFRP bars, and  $\epsilon_{cu}$  is the ultimate strain in concrete (taken as 0.003).

The factor  $\beta_1$  can be calculated using Equation (4).

$$\beta_1 = 0.85 - \frac{0.05(f'_c - 28)}{7} \geq 0.65 \tag{4}$$

The predicted failure mode can be determined with the help of the following failure conditions. If  $(\rho_f < \rho_{fb})$ , then the condition of failure is due to tension. When  $(\rho_{fb} < \rho_f < 1.4*\rho_{fb})$ , the balanced failure condition takes place with the crushing of concrete, followed by the rupture of the GFRP bar, and for  $(\rho_f > 1.4*\rho_{fb})$ , the RC element fails due to compression failure. From the above conditions, all of the tested concrete slabs reinforced with GFRP rods failed due to compression failure. As  $\rho_f > \rho_{fb}$ , the slab is considered over-reinforced, the controlling limit state is the crushing of concrete, and the moment of resistance ( $M$ ) can be calculated using Equation (5).

$$M = \rho_f f_f b d_2 \left( 1 - 0.59 \frac{\rho_f f_f}{f'_c} \right) \tag{5}$$

where  $f_f$  is the tensile strength of the GFRP rods, and  $f_f$  can be calculated using Equation (6).

$$f_f = \sqrt{\frac{(E_f \epsilon_{cu})^2}{4} + \frac{0.85 \beta_1 f'_c}{\rho_f} E_f \epsilon_{cu} - 0.5 E_f \epsilon_{cu}} \leq f_{fu} \tag{6}$$

The moment resistance of the GRC and GRF slab specimens was obtained using ACI 440.1R-15, and the results are shown in Table 7. The theoretical moment of resistance obtained by slabs reinforced with GFRP rods is 4.48 kNm.

**Table 7.** Comparison of the moment of resistance for slabs reinforced with GFRP rods.

Specimen	Reinforcement Ratio ( $\rho_f$ )	Failure Mode	Moment of Resistance		Percentage of Deviation (%)
			M,Exp (kN·m)	M,ACI (kN·m)	
GRC 1	$1.44\rho_{fb}$	Compression failure	3.87	4.48	15.9
GRC 2	$1.44\rho_{fb}$	Compression failure	3.75	4.48	19.6
GRF 1	$1.44\rho_{fb}$	Compression failure	4.24	4.48	5.84
GRF 2	$1.44\rho_{fb}$	Compression failure	4.04	4.48	11.0

#### 4.2. Comparison of Experimental Results with Theoretical Predictions

The moment of resistance ( $M$ ) of the slab reinforced with GFRP rods was calculated using ACI 440.1R-15, and experimental results are shown in Table 7. The moment of resistance calculated using ACI 440.1R-15 overestimated the ultimate moment carrying capacity of OPC/fly ash concrete slabs reinforced with GFRP bars by 17.81% and 8.46%, respectively. Figure 15 shows a graphical comparison of the moment of resistance predicted by ACI 440.1R 15 and experimental results.

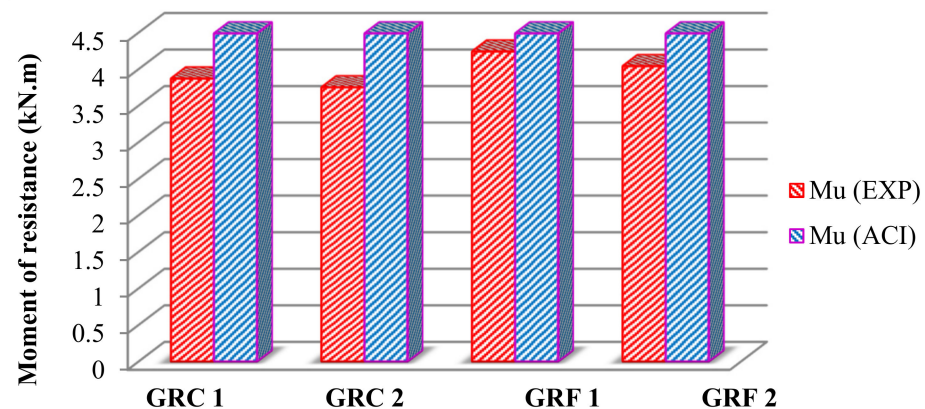


**Figure 15.** Moment of resistance of GFRP slabs.

### 5. Nonlinear Finite Element Analysis (NLFEA)

Nonlinear finite element analysis (NLFEA) was carried out using the ANSYS 2022-R1 [38] software, and the results were compared with the experimental results. From the experimental study, it was found that the fly ash concrete slab reinforced with GFRP rods has a higher load-carrying capacity than the other slab specimens. Therefore, the slab specimens SRF and GRF were considered for the finite element analysis.

#### 5.1. Modeling

For modeling the concrete, the SOLID-65 element was used, which is an eight-noded solid element with three degrees of freedom at each node. For modeling the steel/GFRP rod, LINK-180, a two-noded element, was used. The support and the loading conditions of the model were created following the experimental setup, as shown in Figure 16.

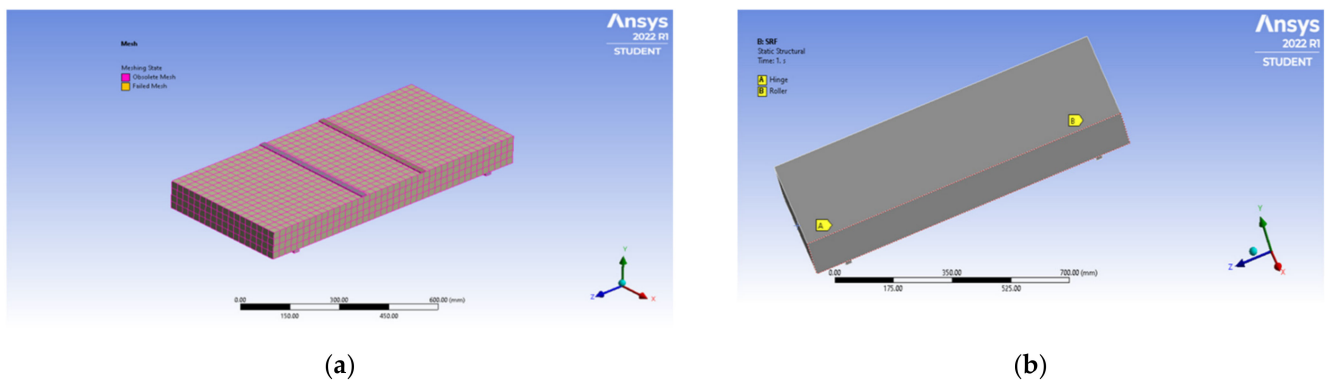


Figure 16. Slab model in ANSYS 2022-R1: (a) meshed model; (b) support conditions.

The ultimate deflections of the SRF and GRF slabs are shown in Figures 17 and 18, respectively. The ultimate loads of the slab specimens SRF and GRF were 27 kN and 30 kN, respectively, with ultimate deflections of 16.4 mm and 12.3 mm.

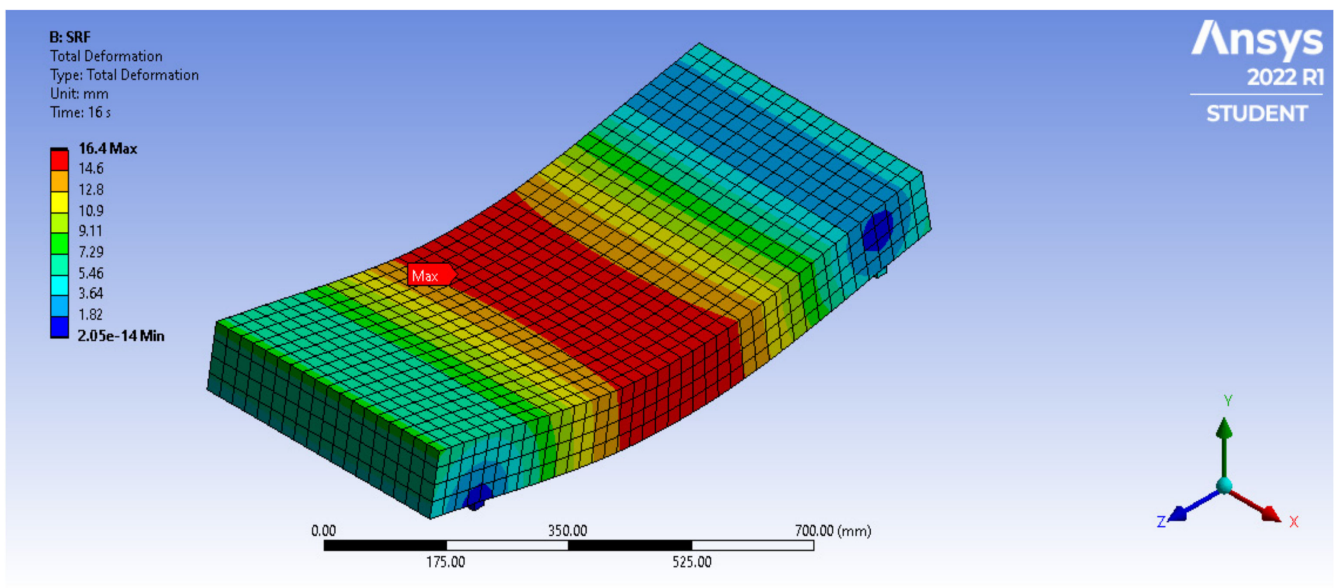


Figure 17. Ultimate deflection of SRF slab.

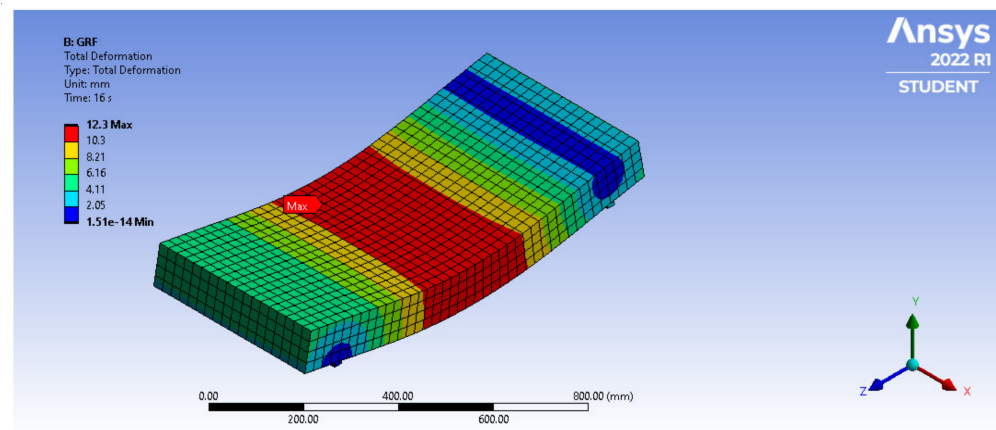


Figure 18. Ultimate deflection of GRF slab.

5.2. Comparison of Experimental Results with NLFEA Results

The comparison of experimental results with NLFEA results is shown in Table 8. The deviations of ultimate load and ultimate deflection from the experimental values are less than 10% for both the SRF and GRF slabs. Hence, ANSYS 2022-R1 [38] software can be used for the analysis of fly ash concrete slabs reinforced with GFRP bars. Figure 19 shows the comparison of the load–deflection behaviors of the SRF and GRF slabs obtained from the NLFEA to the experimental results. From the results, it is observed that both the experimental and numerical results are in good agreement.

Table 8. Comparison between experimental and numerical results.

Specimen Id.	Ultimate Load (kN)		Deflection at Mid-Span (mm)	
	Experimental	NLFEA (ANSYS)	Experimental	NLFEA (ANSYS)
SRF	28.5	27	17.9	16.4
GRF	31.8	30	13.6	12.3

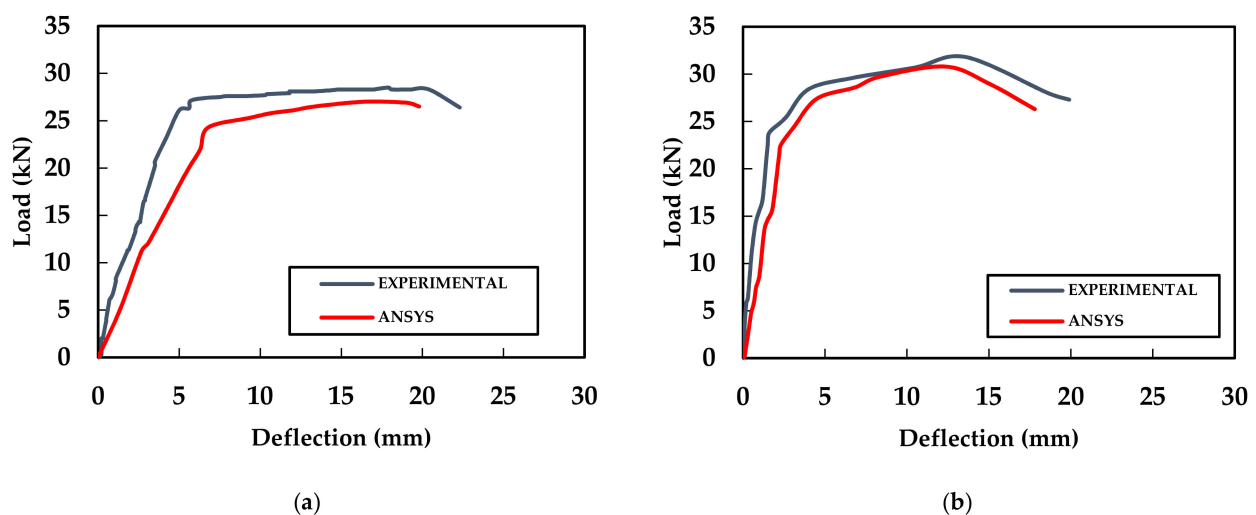


Figure 19. Comparison between experimental and numerical load–deflection behavior of (a) SRF and (b) GRF.

6. Conclusions

From this study, the following observations and conclusions can be made based on experiments conducted on OPC/fly ash concrete slabs reinforced with steel/GFRP bars.

1. The slab specimens SRF, GRC, and GRF showed 17%, 19%, and 30% increases in their ultimate load-carrying capacity when compared with the control specimen SRC.
2. The concrete surface strain was slightly higher for the fly ash concrete slab than for the OPC concrete slab, and the strain value of GFRP bars was higher than that of steel bars under the same loading. This shows that the flexural strength of the GFRP-reinforced concrete slab is higher than that of the steel-reinforced concrete slab.
3. The ultimate moment capacity of the GRF slab was 12% higher than that of the SRF slab, and the ultimate moment capacity of the GRC slab was 20% higher than that of the SRC slab. The slabs reinforced with GFRP rods are capable of exhibiting more curvature before failure when compared to the slabs reinforced with steel.
4. The average ductility of the steel rod was higher than that of the GFRP rod. Both the steel- and GFRP-reinforced slabs failed due to flexure with maximum strength and ductility.
5. The analytical equations given by ACI 440.1R-15 for calculating the moment of resistance overestimated the experimental results by 18%. Thus, ACI 440.1R-15 can be used for the design of concrete slabs reinforced with GFRP rods.
6. Only 10% deviation was observed between the experimental and the nonlinear finite element analysis (NLFEA) results. Hence, ANSYS 2022-R1 software can be used for the analysis of fly ash concrete slabs reinforced with GFRP bars.

Thus, it is observed that GFRP rods, when used as a replacement for steel rods in both conventional and fly ash concrete, provide improved strength compared to the one-way slab. In addition, the slabs reinforced with GFRP rods did not exhibit sudden failure, even though GFRP rods are brittle. The results of this investigation demonstrate the ability and the potential use of GFRP rods with fly ash concrete in slab elements.

**Author Contributions:** C.S.M. and S.M.: Conceptualized the model, established the empirical theorem, and conducted the experiments. P.S.J., B.G.A.G. and K.R.: Supervised the research as well as the analysis of results. P.S.J., C.S.M. and S.M.: Introduced the idea of static loading in this project, designed the slab, wrote, reviewed, and submitted the paper, and collaborated in and coordinated the research. P.S.J., B.G.A.G. and K.R.: Suggested and chose the journal for submission. P.S.J., B.G.A.G. and K.R.: Participated in the manuscript revision phase. All authors have read and agreed to the published version of the manuscript.

**Funding:** This research received no external funding.

**Institutional Review Board Statement:** Not applicable.

**Informed Consent Statement:** Not applicable.

**Data Availability Statement:** The data presented in this study are available on request from the corresponding author.

**Conflicts of Interest:** This manuscript has not been submitted to, nor is it under review by, another journal or other publishing venue. The authors have no affiliation with any organization with a direct or indirect financial interest in the subject matter discussed in the manuscript. The authors declare no conflict of interest.

## References

1. Liew, K.; Sojobi, A.; Zhang, L. Green concrete: Prospects and challenges. *Constr. Build. Mater.* **2017**, *156*, 1063–1095. [[CrossRef](#)]
2. Barbuta, M.; Bucur, R.; Serbanoiu, A.; Scutarasu, S.; Burlacu, A. Combined Effect of Fly Ash and Fibers on Properties of Cement Concrete. *Procedia Eng.* **2017**, *181*, 280–284. [[CrossRef](#)]
3. Siddique, R. Effect of fine aggregate replacement with Class F fly ash on the mechanical properties of concrete. *Cem. Concr. Res.* **2003**, *33*, 539–547. [[CrossRef](#)]
4. Detwiler, R.J. *Substitution of Fly Ash for Cement or Aggregate in Concrete: Strength Development and Suppression of ASR*; RD127; Portland Cement Association: Skokie, IL, USA, 2002.
5. Siddique, R. Performance characteristics of high-volume Class F fly ash concrete. *Cem. Concr. Res.* **2004**, *34*, 487–493. [[CrossRef](#)]
6. Joanna, P.S.; Rooby, J.; Prabhavathy, A.; Preetha, R.; Pillai, C.S. Behaviour of reinforced concrete beams with 50 percentage fly ash international journal of civil engineering and technology. *Int. J. Civ. Eng. Technol.* **2013**, *4*, 36–48.
7. Malhotra, V.M. High-Performance, High Volume FlyAsh Concrete. *Concr. Int.* **2002**, *24*, 30–34.

8. Saha, A. Effect of class F fly ash on the durability properties of concrete. *Sustain. Environ. Res.* **2018**, *28*, 25–31. [[CrossRef](#)]
9. Thomas, M.D.A. *Optimizing the Use of Fly Ash in Concrete*; Portland Cement Association: Skokie, IL, USA, 2007.
10. Murali, M.; Mohammed, B.S.; Abdulkadir, I.; Liew, M.S.; Alaloul, W.S. Utilization of Crumb Rubber and High-Volume Fly Ash in Concrete for Environmental Sustainability: RSM-Based Modeling and Optimization. *Materials* **2021**, *14*, 3322. [[CrossRef](#)]
11. Hu, W.; Li, Y.; Yuan, H. Review of Experimental Studies on Application of FRP for Strengthening of Bridge Structures. *Adv. Mater. Sci. Eng.* **2020**, *2020*, 8682163. [[CrossRef](#)]
12. Mertol, H.C.; Rizkalla, S.; Scott, P.; Lees, J.M.; El-Hachal, R. Durability of concrete beams prestressed with CFRP. *Symp. Pap.* **2007**, *245*, 1–20.
13. Shave, J. The time has come for high strength, low maintenance fibre reinforced plastics. *New Civil Eng.* **2014**, *11*.
14. Yooprasertchai, E.; Dithaem, R.; Arnamwong, T.; Sahamitmongkol, R.; Jadekittichoke, J.; Joyklad, P.; Hussain, Q. Remediation of Punching Shear Failure Using Glass Fiber Reinforced Polymer (GFRP) Rods. *Polymers* **2021**, *13*, 2369. [[CrossRef](#)] [[PubMed](#)]
15. Mussa, M.H.; Radzi, N.A.M.; Hamid, R.; Mutalib, A.A. Fire Resistance of High-Volume Fly Ash RC Slab Inclusion with Nano-Silica. *Materials* **2021**, *14*, 3311. [[CrossRef](#)] [[PubMed](#)]
16. Zaghoul, M.M.Y.; Mohamed, Y.S.; El-Gamal, H. Fatigue and tensile behaviors of fiber-reinforced thermosetting composites embedded with nanoparticles. *J. Compos. Mater.* **2018**, *53*, 709–718. [[CrossRef](#)]
17. Zaghoul, M.M.Y.; Steel, K.; Veidt, M.; Heitzmann, M.T. Wear behaviour of polymeric materials reinforced with man-made fibres: A comprehensive review about fibre volume fraction influence on wear performance. *J. Reinf. Plast. Compos.* **2022**, *41*, 215–241. [[CrossRef](#)]
18. Zaghoul, M.M.Y.; Zaghoul, M.M.Y. Influence of flame retardant magnesium hydroxide on the mechanical properties of high density polyethylene composites. *J. Reinf. Plast. Compos.* **2017**, *36*, 1802–1816. [[CrossRef](#)]
19. Zaghoul, M.Y.M.; Zaghoul, M.M.Y.; Zaghoul, M.M.Y. Developments in polyester composite materials—An in-depth review on natural fibres and nano fillers. *Compos. Struct.* **2021**, *278*, 114698. [[CrossRef](#)]
20. Mohamed, Y.S.; El-Gamal, H.; Zaghoul, M.M.Y. Micro-hardness behavior of fiber reinforced thermosetting composites embedded with cellulose nanocrystals. *Alex. Eng. J.* **2018**, *57*, 4113–4119. [[CrossRef](#)]
21. Zaghoul, M.M.Y.M. Mechanical properties of linear low-density polyethylene fire-retarded with melamine polyphosphate. *J. Appl. Polym. Sci.* **2018**, *135*, 46770. [[CrossRef](#)]
22. Zaghoul, M.M.Y.; Zaghoul, M.Y.M.; Zaghoul, M.M.Y. Experimental and modeling of mechanical-electrical behavior of polypropylene composites filled with graphite and MWCNT fillers. *Polym. Test.* **2017**, *63*, 467–474. [[CrossRef](#)]
23. Bedon, C.; Louter, C. Structural glass beams with embedded GFRP, CFRP or steel reinforcement rods: Comparative experimental, analytical and numerical investigations. *J. Build. Eng.* **2019**, *22*, 227–241. [[CrossRef](#)]
24. Jalal, A.; Hakim, L.; Shafiq, N. Mechanical and Post-Cracking Characteristics of Fiber Reinforced Concrete Containing Copper-Coated Steel and PVA Fibers in 100% Cement and Fly Ash Concrete. *Appl. Sci.* **2021**, *11*, 1048. [[CrossRef](#)]
25. *ACI 440.1R-15*; Guide for the Design and Construction of Concrete Reinforced with Fiber Reinforced Polymers (FRP) Bars; American Concrete Institute: Farmington Hills, MI, USA, 2015.
26. Balendran, R.; Rana, T.; Maqsood, T.; Tang, W. Application of FRP bars as reinforcement in civil engineering structures. *Struct. Surv.* **2002**, *20*, 62–72. [[CrossRef](#)]
27. Balafas, I.; Burgoyne, C. Economic design of beams with FRP rebars or prestress. *Mag. Concr. Res.* **2012**, *64*, 885–898. [[CrossRef](#)]
28. Hollaway, L. A review of the present and future utilisation of FRP composites in the civil infrastructure with reference to their important in-service properties. *Constr. Build. Mater.* **2010**, *24*, 2419–2445. [[CrossRef](#)]
29. Jabbar, S.; Farid, S. Replacement of steel rebars by GFRP rebars in the concrete structures. *Karbala Int. J. Mod. Sci.* **2018**, *4*, 216–227. [[CrossRef](#)]
30. Kemp, M.; Blowes, D. Concrete Reinforcement and Glass Fibre Reinforced Polymer. *Qld. Roads Ed.* **2011**, *11*, 40–48.
31. Borosnyói, A. Corrosion-resistant concrete structures with innovative Fibre Reinforced Polymer (FRP) materials. *Epa.-J. Silic. Based Compos. Mater.* **2013**, *65*, 26–31.
32. Sólyom, S.; Balázs, G.L.; Borosnyói, A. Material characteristics and bond tests for FRP rebars. *Concr. Struct.* **2015**, *16*, 38–45.
33. Patil, V.R. Experimental Study of Behavior of RCC Beam by Replacing Steel Bars with Glass Fiber Reinforced Polymer and Carbon Reinforced Fiber Polymer (GFRP). *Int. J. Innov. Res. Adv. Eng.* **2014**, *1*, 205–210.
34. Goonewardena, J.; Ghabraie, K.; Subhani, M. Flexural Performance of FRP-Reinforced Geopolymer Concrete Beam. *J. Compos. Sci.* **2020**, *4*, 187. [[CrossRef](#)]
35. Adam, M.A.; Erfan, A.M.; Habib, F.A.; El-Sayed, T.A. Structural Behavior of High-Strength Concrete Slabs Reinforced with GFRP Bars. *Polymers* **2021**, *13*, 2997. [[CrossRef](#)] [[PubMed](#)]
36. Jayajothi, P.; Kumutha, R.; Vijai, K. Finite element analysis of FRP strengthened RC beams using Ansys. *Asian J. Civ. Eng.* **2013**, *14*, 631–642.
37. Gherbi, A.; Dahmani, L.; Boudjemia, A. Study on two way reinforced concrete slab using Ansys with different boundary conditions and loading world academy of science. *Eng. Technol. Int. J. Civ. Environ. Eng.* **2018**, *12*, 1151–1156.
38. *ANSYS 2022-R1*; Manual Set. ANSYS Inc.: Canonsburg, PA, USA, 2022.
39. Gu, H.S.; Zhu, D.Y. Flexural Behaviours of Concrete Slab Reinforced with GFRP bars. *Adv. Mater. Res.* **2011**, *243–249*, 567–572. [[CrossRef](#)]



40. Moon, J.; Reda Taha, M.M.; Kim, J.J. Flexural Strengthening of RC Slabs Using a Hybrid FRP-UHPC System Including Shear Connector. *Adv. Mater. Sci. Eng.* **2017**, *2017*, 4387545. [[CrossRef](#)]
41. Dhipanaravind, S.; Sivagamasundari, R. Flexural Behaviour of Concrete One-way Slabs Reinforced with Hybrid FRP Bars. *Int. J. Appl. Eng.* **2018**, *13*, 4807–4815.
42. Venkatesan, G.; Raman, S.R.; Sekaran, M.C. Flexural behaviour of reinforced concrete beams using high volume fly ash concrete confinement in compression zone. *J. Civ. Eng. (IEB)* **2013**, *41*, 87–97.
43. El Zareef, M.; El Madawy, M. Effect of glass-fiber rods on the ductile behaviour of reinforced concrete beams. *Alex. Eng. J.* **2018**, *57*, 4071–4079. [[CrossRef](#)]
44. Thamrin, R.; Zaidir, Z.; Iwanda, D. Ductility Estimation for Flexural Concrete Beams Longitudinally Reinforced with Hybrid FRP–Steel Bars. *Polymers* **2022**, *14*, 1017. [[CrossRef](#)]
45. Gunes, O.; Lau, D.; Tuakta, C.; Büyüköztürk, O. Ductility of FRP–concrete systems: Investigations at different length scales. *Constr. Build. Mater.* **2013**, *49*, 915–925. [[CrossRef](#)]
46. Ahmed, H.; Jaf, D.; Yaseen, S. Comparison of the Flexural Performance and Behaviour of Fly-Ash-Based Geopolymer Concrete Beams Reinforced with CFRP and GFRP Bars. *Adv. Mater. Sci. Eng.* **2020**, *2020*, 3495276. [[CrossRef](#)]